

# Charge Transport Mechanism and Trap Origin in Methyl-Terminated Organosilicate Glass Low- $\kappa$ Dielectrics

Timofey V. Perevalov,\* Andrei A. Gismatulin, Andrei E. Dolbak, Vladimir A. Gritsenko, Elena S. Trofimova, Vladimir A. Pustovarov, Dmitry S. Seregin, Konstantin A. Vorotilov, and Mikhail R. Baklanov

The charge transport and trap nature responsible for the leakage current through thermally cured methyl-terminated organosilicate low- $\kappa$  dielectric films are studied. It is found that the Frenkel emission does not describe correctly the charge transport in the studied films. The charge transport occurs via the phonon-assisted electron tunneling between neutral traps as described in the Nasyrov–Gritsenko model. The obtained thermal trap energy value 1.2 eV is close to that for the oxygen divacancy (Si–Si–Si cluster) in SiO<sub>2</sub>. The electron energy loss spectra, photoluminescence excitation of 2.7 eV blue band spectra, and data from the simulation within the density functional theory for the model SiCOH low- $\kappa$  structure confirm the presence of oxygen vacancy and divacancy in the studied films. The thermal trap energy value estimated as half the Stokes shift of the blue luminescence also gives a value close to 1.2 eV. It proves the correctness of the Nasyrov–Gritsenko model for describing the charge transport mechanism and the conclusion that oxygen divacancies are traps responsible for the leakage current in the studied low- $\kappa$  films.

## 1. Introduction

The signal propagation delay in interconnects (RC delay) is a serious obstacle to the continued scaling of ultra large scale integration (ULSI) devices. The total resistance ( $R$ ) of conductive wires in the interconnect structure and capacitance ( $C$ ) between the wires are the factors significantly affecting the chip performance.<sup>[1]</sup> The replacement of traditional Al by low-resistivity conductors (Cu, Co, etc.) has decreased the interconnect RC delay and increased the IC (integrated circuit) speed. Various low-dielectric-constant materials (low- $\kappa$ ), from organic polymers to zeolites and metal-organic frameworks, were being evaluated as possible candidates for ULSI interconnects during the last two decades. Most of them demonstrated challenges making them hardly compatible with the

existing ULSI technology.<sup>[2]</sup> At the end, organosilicate glasses (OSGs, e.g., SiCOH) were selected for the interconnect technology because they have properties similar to those of traditional SiO<sub>2</sub>, use the same technological equipment, and have better compatibility with damascene integration technology. OSG films are deposited by using a mixture of a matrix-forming precursors and porogen. In plasma enhanced chemical vapor deposition (PECVD), the porogens are normally sacrificial organic polymers ( $\alpha$ -terpinene, epoxyhexane, nonbornene, and others).<sup>[3]</sup> Spin-on deposition uses self-assembling or nanoclustering techniques. The most advanced spin-on deposition is based on the so-called evaporation induced self-assembling (EISA) technique,<sup>[4]</sup> in which the selected porogen templates (surfactants) are introduced into the solution together with the matrix precursor. The template molecules are self-organized during the solvent evaporation and form micelles. Then they are codeposited together with the matrix precursor and form ordered porosity after thermal removal (curing).<sup>[5]</sup> The matrix has a silica-like structure, in which some bridging oxygen atoms are replaced by terminal (methyl) groups and/or bridging hydrocarbon groups (Figure 1). The curing can also be assisted by UV photons and e-beams that significantly improve the porogen decomposition rate. The terminal methyl groups are needed to keep low- $\kappa$  hydrophobicity,<sup>[6]</sup> while the bridging organic groups improve the mechanical properties of the OSG films.<sup>[7,8]</sup> Carbon-bridged films also need to contain a certain amount of

Dr. T. V. Perevalov, A. A. Gismatulin, Dr. A. E. Dolbak, Dr. V. A. Gritsenko  
Rzhanov Institute of Semiconductor Physics  
SB RAS  
13 Lavrentiev Avenue, 630090 Novosibirsk, Russia  
E-mail: timson@isp.nsc.ru


Dr. T. V. Perevalov, Dr. V. A. Gritsenko  
Novosibirsk State University  
2 Pirogov Street, 630090 Novosibirsk, Russia

Dr. V. A. Gritsenko  
Novosibirsk State Technical University  
20 Marks Avenue, 630073 Novosibirsk, Russia

Dr. E. S. Trofimova, Dr. V. A. Pustovarov  
Ural Federal University  
19 Mira Street, 620002 Ekaterinburg, Russia

Dr. D. S. Seregin, Dr. K. A. Vorotilov, Prof. M. R. Baklanov  
MIREA  
Russian Technological University  
78 Vernadsky Avenue, 119454 Moscow, Russia

Prof. M. R. Baklanov  
North China University of Technology  
5 Jinyuanzhuang Road, Shijingshan District, Beijing 100144, China

 The ORCID identification number(s) for the author(s) of this article can be found under <https://doi.org/10.1002/pssa.202000654>.

DOI: 10.1002/pssa.202000654

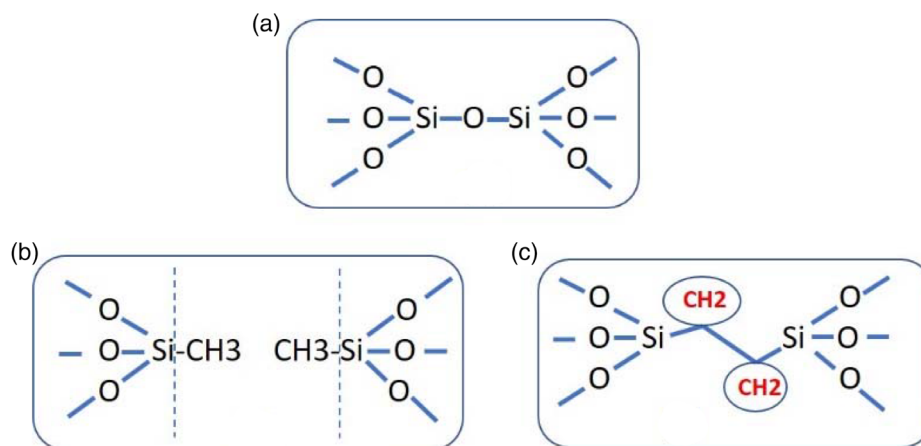


**Figure 1.** Schematic presentation of a) stoichiometric SiO<sub>2</sub> and b) methyl-terminated and c) ethylene-bridged OSG low- $\kappa$  films.

terminal groups to provide sufficient hydrophobicity to low- $\kappa$  films that are introduced by the precursor optimization or by additional silylation after the deposition.<sup>[9]</sup> The porogen removal occurs through the polymer fragmentation with the formation of volatile species, but the process should be sufficiently gentle to avoid significant destruction of SiCH<sub>3</sub> bonds in the matrix. UV photons may also have negative impacts on the electrical properties of the films. First of all, the porogen fragmentation can form the so-called porogen residues, which are amorphous carbon-like compounds.<sup>[10,11]</sup> Their presence in a low- $\kappa$  film significantly increases the leakage current and reduces the breakdown field.<sup>[12]</sup> UV/VUV photons can also influence the most essential electric characteristics of low- $\kappa$  dielectrics, such as permittivity,<sup>[13]</sup> trapped charges,<sup>[14]</sup> leakage currents,<sup>[15,16]</sup> and the breakdown behavior<sup>[17]</sup> without visible chemical or structural changes in OSG. These and other UV radiation-related phenomena were described and discussed in many original publications, which have been systemized and analyzed in detail in a recently published review article.<sup>[18]</sup> Finally, to summarize available experimental data, different leakage current enhancement mechanisms can be considered. The task of analyzing the mechanism becomes even more complicated when using UV curing, as well as in the presence of different carbon groups in the dielectric.

To identify the ways of improving the electrophysical properties of low- $\kappa$  dielectrics, it is important to know the charge current mechanism and trap nature responsible for their leakage current. The charge transport mechanism in PECVD low- $\kappa$  dielectrics with terminal methyl groups was studied previously.<sup>[2,19–22]</sup> However, the consideration of this issue, in most cases, is limited to the use of the Frenkel mechanism, but more accurate and complex models, such as phonon-assisted tunneling between neutral traps and multiphonon ionization of neutral traps, are not considered. In fact, the Frenkel mechanism can describe the charge transport of many dielectrics only formally, with greatly underestimated pre-exponential frequency factor values.

In this work, OSG (SiCOH) low- $\kappa$  films containing only terminal methyl groups are investigated. Unlike previous publications on charge transfer mechanisms, only thermally cured (no UV radiation) films are investigated. This reduces the

uncertainties related to UV photon effects, especially associated with the formation of conductive porogen residues. Thus, we analyze the most important factors responsible for the charge transport in methyl-terminated OSG low- $\kappa$  films.

## 2. Experimental Section

The film-forming solutions were prepared by mixing tetraethyl orthosilicate (TEOS; Si(C<sub>2</sub>H<sub>5</sub>O)<sub>4</sub>; 99.999%, Sigma-Aldrich) and methyltriethoxysilane (MTEOS; CH<sub>3</sub>Si(C<sub>2</sub>H<sub>5</sub>O)<sub>3</sub>; 99%, Sigma-Aldrich), 2-propanol, Honeywell semiconductor grade VLSI) in the presence of catalyst HCl (37%, Sigma-Aldrich) in the ratio [Si(C<sub>2</sub>H<sub>5</sub>O)<sub>4</sub> + CH<sub>3</sub>Si(C<sub>2</sub>H<sub>5</sub>O)<sub>3</sub>]/H<sub>2</sub>O/HCl = 1/4/0.002 to provide proper hydrolysis conditions.<sup>[23]</sup> The mixture was warmed up at 60 °C for 3 h under constant stirring. The curing time was optimized to reduce the amount of remaining carbon residues that could be formed during the template destruction, but the concentration of Si–CH<sub>3</sub> groups was kept sufficient to avoid the formation of SiOH groups and further moisture adsorption.

The films were spin-on deposited on phosphorus-doped Si (100) wafers with resistivity 50 ohm cm at the rotation speed 2500 rpm with the use of a WS-650-8NPP (Laurell). To create a porous structure, the EISA process was used.<sup>[4]</sup> In this process, the surfactant was added to the solution and the organic mesophase precipitated in silica matrix issued during the spin-on deposition. The nonionic surfactant BrijL4 (polyethylene glycol dodecyl ether C<sub>12</sub>H<sub>25</sub>(OCH<sub>2</sub>OCH<sub>2</sub>)<sub>4</sub>OH, molar mass 362 g mol<sup>−1</sup>, Sigma-Aldrich) was used as a self-assembled agent. Its concentration was BrijL4/(TEOS + MTEOS + BrijL4) = 17.5 wt%. The deposited films were immediately cured by a hot plate at Ta = 200 °C, 10 min (soft bake), and annealed in air at Ta = 430 °C, 30 min (hard bake). According to the measurements conducted by ellipsometric porosimetry, the open porosity of the fully cured films was close to 40%. The terminal groups were preferentially located on the pore wall.<sup>[24]</sup>

The condensation of hydroxyl groups causes the formation of a Si–O network, whereas terminal methyl groups do not undergo hydrolysis and do not participate in the condensation process. As a result, the Si–O network with methyl terminal

groups is formed. The Si/CH<sub>3</sub> ratio of in the films was ≈0.6. This composition was chosen to provide a compromise between the dielectric constant and Young's modulus.<sup>[9]</sup> The 203 nm thick films with refractive index 1.246 (±0.004) and a full porosity of ≈43% were used for electric measurements.

The metal–dielectric–semiconductor structure fabrication included the deposition of a continuous Al contact on the back side of the Si substrate, and a  $5 \times 10^{-3} \text{ cm}^2$  magnesium contact was sputtered on top of the low- $\kappa$  film using a shadow mask. To remove the adsorbed impurities, the samples were annealed for 30 min at 300 °C in an Ar atmosphere before the metal contact deposition. The current–voltage ( $I$ – $V$ ) characteristics at different temperatures were measured at a negative potential on the metal using the Keithley 2400 equipment. The voltage rise rate, when measuring the  $I$ – $V$  characteristics, was  $0.9 \text{ V s}^{-1}$ .  $I$ – $V$  characteristics were investigated at the applied field below  $2 \text{ MV cm}^{-1}$  because at a higher value, the stress-induced leakage current (SILC) effect occurs.

The electron energy loss spectra (EELS) were obtained by using the Riber LAS-2000 spectrometer. The incident electron beam energy was 200 eV. The amplitude of the modulation signal for the synchronous detector was 0.3 V.

The photoluminescence (PL) spectra and PL excitation (PLE) spectra under UV–VUV excitation were measured in the Institute of Physics, University of Tartu, using a 150 W deuterium discharge lamp Hamamatsu L1835 and a McPherson 234/302 monochromator. The grating monochromator Andor SR 303i-B equipped with a H8259-01 photon counting head was used to select the emission. Various color glass filters, provided by SHCOTT and UQG Optics, were used to suppress the effects of second orders of excitation or emission and stray light. The samples were mounted in a closed cycle helium cryostat provided by ARS (Advanced Research System, Inc) designed for low-temperature measurements (5 K). The measurements were fully controlled by using a LabView-based software. All PL spectra were corrected for the spectral sensitivity of the detection systems. The PLE spectrum was corrected for the wavelength-dependent photon flux variation using sodium salicylate.

The ab initio simulation of electronic structure was conducted within density functional theory (DFT) in the 3D periodic supercell model with the plane wave basis and optimized norm-conserving Vanderbilt pseudopotential in the Quantum ESPRESSO package.<sup>[25]</sup> The hybrid exchange–correlation functional PBE0 was used. The low- $\kappa$  SiCOH model structure was obtained as follows. First, a Si<sub>12</sub>O<sub>24</sub> supercell of  $\beta$ -cristobalite (as it closest to amorphous structure) was obtained. Second, the two adjacent tetrahedra SiO<sub>4</sub> were removed from that supercell. Third, six methyl groups (CH<sub>3</sub>) were added to the pore. Fourth, full structural relaxation was made. Thus, 64 structures with different initial positions and orientations of CH<sub>3</sub> were calculated, and a structure with the minimal total energy was selected. The obtained structure is shown in **Figure 2**. This model structure is remarkable for its simplicity (51 atoms in a cell only). It has the Si/CH<sub>3</sub> ratio 0.6 for studied films and it contains all the essential structural units. The validity of this structure was confirmed by reasonable calculated mass density ( $1.75 \text{ g cm}^{-3}$ ) and relatively low dielectric permittivity (3.5) and bandgap (7.0 eV) values. The electronic structure of oxygen vacancy and divacancy was simulated for the 102-atom supercell

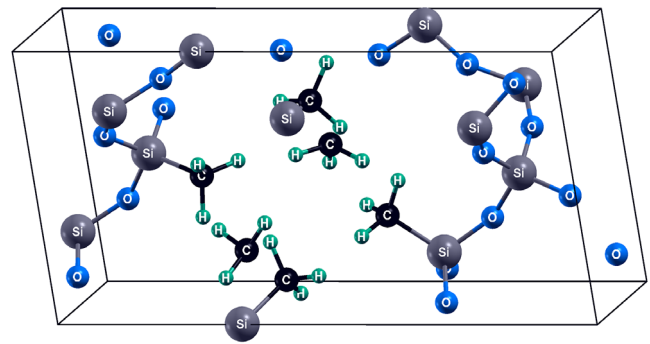


**Figure 2.** SiCOH methyl-terminated low- $\kappa$  model structure used for ab initio simulation.

that was created by the  $1 \times 2 \times 1$  translation of a 51-atom cell. All nonequivalent defect positions were considered.

### 3. Results and Discussion

First of all, we investigated the current–voltage characteristics, measured at different temperatures, of the studied low- $\kappa$  dielectric (**Figure 3**). The  $I$ – $V$  characteristics were analyzed in the frame of the Frenkel mechanism<sup>[26]</sup> that is commonly used to

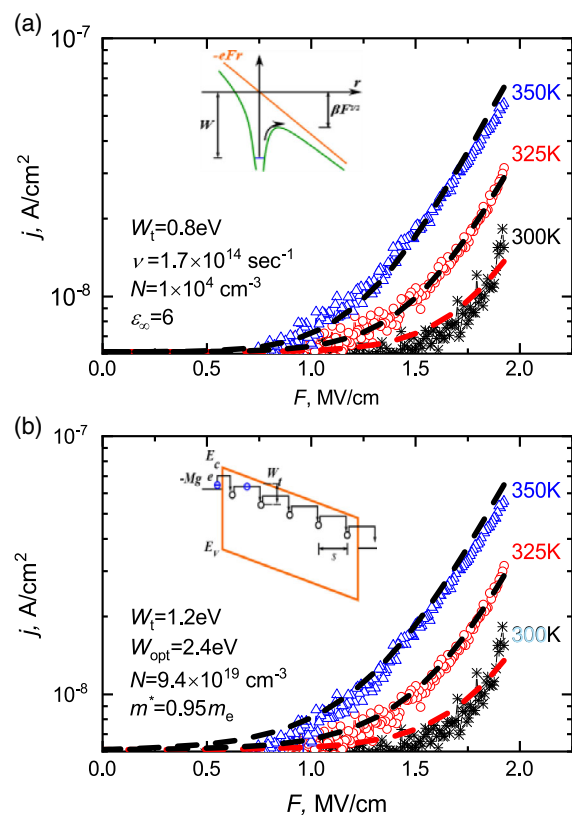


**Figure 3.**  $I$ – $V$  characteristics of low- $\kappa$  dielectric: experiment—characters, simulation within a) Frenkel model and b) the Nasyrov–Gritsenko model—dashed lines. The fitting parameters of the models are inserted in the figures.

describe the dielectric conductivity, and by the Nasyrov–Gritsenko (N–G) model<sup>[27,28]</sup> of the phonon-assisted tunneling between neutral traps, which is a more complex and flexible model. For completeness, the Hill–Adachi (H–A) model<sup>[29,30]</sup> of overlapping Coulomb traps and the Makram-Ebeid and Lannoo (ME–L) model<sup>[31]</sup> of isolated trap ionization were also analyzed.

The Frenkel conduction mechanism consists of thermal ionization of an isolated Coulomb trap in an electric field that reduces the energy barrier.<sup>[26]</sup> It is described by the equation

$$J = eN^{2/3}P, \quad P = \nu \exp\left(-\frac{W - \beta_F \sqrt{F}}{kT}\right), \quad (1)$$

$$\beta_F = \left(\frac{e^3}{\pi \epsilon_\infty \epsilon_0}\right)^{1/2}, \quad \nu = W/h$$

In the N–G model, the charge transport involves the trapped electron excitation due to the phonon absorption and its subsequent tunneling to a neighboring neutral trap without excitation to the conduction band (inset in Figure 3b).<sup>[27,28]</sup> The electron tunnels to a neighboring trap due to the large overlap integral. The trap ionization probability  $P$  in the N–G model is given by expression (2)

$$P = \frac{2\sqrt{\pi}\hbar W_t}{m^* s^2 \sqrt{2kT(W_{\text{opt}} - W_t)}} \exp\left(-\frac{W_{\text{opt}} - W_t}{kT}\right) \times \exp\left(-\frac{2s\sqrt{2m^* W_t}}{\hbar}\right) \sinh\left(\frac{eFs}{2kT}\right) \quad (2)$$

In formulas (1) and (2),  $J$  is the current density,  $e$  is the electron charge,  $N = s^{-3}$  is the trap concentration,  $s$  is the average distance between traps,  $\nu = W/h$  is the attempt to escape factor,  $W$  is the trap ionization energy,  $W_t$  is the thermal trap energy,  $W_{\text{opt}}$  is the optical trap energy,  $F$  is the electric field,  $k$  is the Boltzmann constant,  $T$  is temperature,  $\epsilon_\infty$  is the high-frequency dielectric permittivity,  $\epsilon_0$  is the dielectric constant, and  $m^*$  is the electron effective mass.

As one can see, the Frenkel mechanism can formally describe the experimental  $I$ – $V$  characteristic of the studied low- $\kappa$  dielectric at the reasonable value  $W = 0.8$  eV, but at abnormally small  $N_t = 10^4$  cm<sup>-3</sup> and high  $\epsilon_\infty = 6$  values. Therefore, one can say that the Frenkel emission does not describe the charge transport mechanism in the low- $\kappa$  dielectric with methyl-terminated groups. The same conclusion can be drawn on the description of the experimental  $I$ – $V$  characteristic by the H–A and ME–L models. The H–A model gives an abnormally low attempt to escape factor  $\nu = 10^4$  s<sup>-1</sup> value, whereas the ME–L model gives a too high (for the applicability of this model) trap concentration  $N_t = 10^{21}$  cm<sup>-3</sup> value. The Schottky injection model was also excluded because it is a type of Frenkel model but with a four times smaller  $\epsilon_\infty$  value. The N–G model qualitatively describes the  $I$ – $V$  characteristic of the low- $\kappa$  dielectric at reasonable fitting parameter values:  $W_t = 1.2$  eV,  $W_{\text{opt}} = 2.4$  eV,  $m^* = 0.95m_0$ , and  $N_t = 9.4 \times 10^{19}$  cm<sup>-3</sup>. The average distance between traps corresponding to the found trap concentration value is  $N_t^{(-1/3)} = 2.2$  nm. Thus, the charge transport through the studied SiCOH low- $\kappa$  occurs via the phonon-assisted electron tunneling between the neutral traps.

It is worth noting that the charge transport mechanisms in methyl-terminated low- $\kappa$  dielectrics were previously described by the Schottky emission, the Poole–Frenkel emission, and space charge limited current model.<sup>[22,32]</sup> However, those results were obtained within the simulation of current–voltage characteristics at one (room) temperature. In this case, the trap ionization energy is not specific. In addition, the Poole–Frenkel model analysis was conducted without evaluating the pre-exponential attempt to the escape factor value. In turn, the physically relevant value of this parameter is one of the criteria for the applicability of this model.

The obtained trap energy value can be compared with the known trap energy values for SiO<sub>2</sub>. In SiO<sub>2</sub>, oxygen vacancies (Si–Si bonds) and divacancies (Si–Si–Si bonds) act as electron and hole traps. It is reliably established that the oxygen vacancies in SiO<sub>2</sub> are the traps with energy 1.6 eV.<sup>[33]</sup> A trap with an energy of  $\approx 1.2$  eV in SiO<sub>2</sub> is most likely an oxygen divacancy, as it follows from the analysis of oxygen vacancy–related defect center annealing kinetics and thermally stimulated current.<sup>[34,35]</sup> Thus, we can assume that the trap energy value 1.2 eV in the studied SiCOH low dielectric is due to Si–Si–Si oxygen divacancies. This conclusion is consistent with the reported data on the presence of oxygen vacancies in SiCOH low- $\kappa$  dielectrics, which are created during the UV curing process.<sup>[36]</sup>

The silicon atom on the studied films has the tetrahedral coordination, including bridging oxygen atoms and terminal methyl CH<sub>3</sub> groups (Figure 1b). The film fabrication included the codeposition of the matrix materials and sacrificial porogen. The soft anneal at 150–200 °C leads to the nanophase separation forming agglomerated porogen and the first step of matrix crosslinking. The porous structure is formed during the porogen removal and short-ranged structural rearrangement in the matrix at 400–450 °C (hard bake). The short-ranged structural rearrangement occurring during the hard bake includes the condensation reaction of remaining silanol groups (Si–OH + HO–Si → Si–O–Si + H<sub>2</sub>O) and the segregation of methyl groups to the pore wall surface,<sup>[23]</sup> and this process can leave a certain amount of Si dangling bonds (oxygen vacancies) inside the matrix. The recombination of these bonds can form Si–Si vacancies and Si–Si–Si oxygen divacancies that may influence the charge transport. The mechanisms of oxygen vacancy aggregation in SiO<sub>2</sub> were studied extensively and they have been reviewed recently in Gao et al.<sup>[36]</sup> It is shown that a neutral vacancy diffusion barrier is about 4.6 eV<sup>[37]</sup> and, therefore, the clustering of randomly distributed neutral vacancies via diffusion is difficult. However, in the case of OSG low- $\kappa$  films, the vacancies' clustering may proceed when the low- $\kappa$  matrix is still not completely “frozen” and the matrix components have a possibility of relatively easy diffusion.<sup>[38]</sup>

This assumption is indirectly confirmed by our DFT calculations of the simple model low- $\kappa$  dielectric structure, according to which the neutral oxygen divacancy formation energy is close to that for pairs of distanced vacancies, whereas for SiO<sub>2</sub> the oxygen divacancy formation energy is noticeably higher. The minimum neutral oxygen vacancy formation energy, calculated by the standard method in the oxygen-rich limit,<sup>[39]</sup> is 5.49 eV.

The second derivative of the inelastic scattered electrons with the energy of 205 eV (EELS) for the studied films shows a significant peak at 6.8 eV with a shoulder at 7.6 eV (Figure 4).

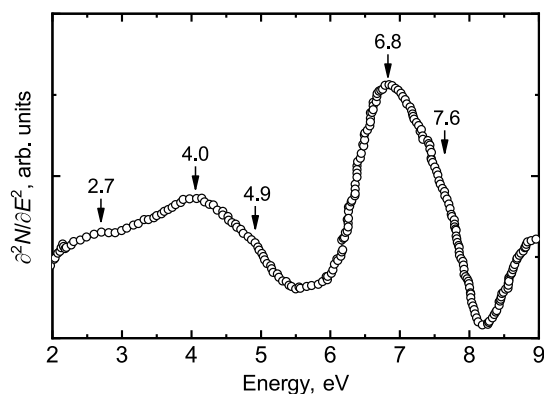


**Figure 4.** EELS of the studied low- $\kappa$  dielectric film.

The excitation at the energy of 7.6 eV is, probably, related to the presence of oxygen vacancies (or Si–Si bonds), as it is true for SiO<sub>2</sub>.<sup>[40–42]</sup> The peak at 6.8 eV could be referred to the oxygen divacancies (or Si–Si–Si bonds) as in SiO<sub>2</sub>.<sup>[42,43]</sup> The observed peaks at the energy range of 2.7–4.9 eV are explained by the electronic transitions onto other oxygen-deficient-type defects, silicon vacancies, or their combination with the organics.<sup>[44,45]</sup> Thus, the features in the spectrum indicate the presence of oxygen vacancies and divacancies in the studied SiCOH low- $\kappa$  films.

The low-temperature PL spectra for the selective excitation by photons of different energies in the UV–VUV ranges are shown in **Figure 5a**. The intensive blue PL band with the maximum of 2.7 eV and a shoulder with an energy of  $\approx 3.6$  eV are observed. Thus, various electron–hole recombination centers are present in the material. The 2.7 eV emission is caused by the oxygen-deficient-type defects (presumably, a triplet-to-singlet transition on the oxygen vacancy) in the films, as it is explained for amorphous SiO<sub>2</sub>.<sup>[41,42,46,47]</sup>

In the PLE spectrum of the 2.7 eV band, one can see three peaks with the maxima at the energy values of 5.2, 6.1, and 6.9 eV (**Figure 5b**). The peak at the energy of 5.2 eV could be caused by the presence of oxygen-deficient centers: namely, oxygen vacancies and divacancies. This interpretation is based on the explanation of the peak at energy values 5.0–5.17 eV in the PLE spectra for the 2.7 eV PL band<sup>[47,48]</sup> and the optical absorption spectra<sup>[40–42,49]</sup> for amorphous SiO<sub>2</sub>. The peak 6.9 eV in the PLE for the studied OSG low- $\kappa$  dielectric can be also explained as oxygen-deficient centers: namely, oxygen divacancy as it is interpreted for the absorption peak near 6.8 eV for SiO<sub>2</sub>.<sup>[42,49,50]</sup> Continuing the analogy with silicon oxide, one can assume that the observed peak at 6.1 eV also could be caused by oxygen vacancies: namely, the  $E'$  center (vacancy with a trapped hole) on the surface.<sup>[42]</sup>

The projected density of states (PDOS) spectra calculated within the DFT for the model low- $\kappa$  structure for atoms forming Si–Si and Si–Si–Si defects exhibit a filled defect level near the valance band top and an empty one near the conduction band bottom (**Figure 6**). The energies of possible optical transitions between these levels are 7.5 and 6.1 eV for Si–Si and Si–Si–Si defects, respectively. Peaks with these energies are clearly visible in the corresponding optical absorption spectra. The energy of the absorption peak for the oxygen vacancy is close

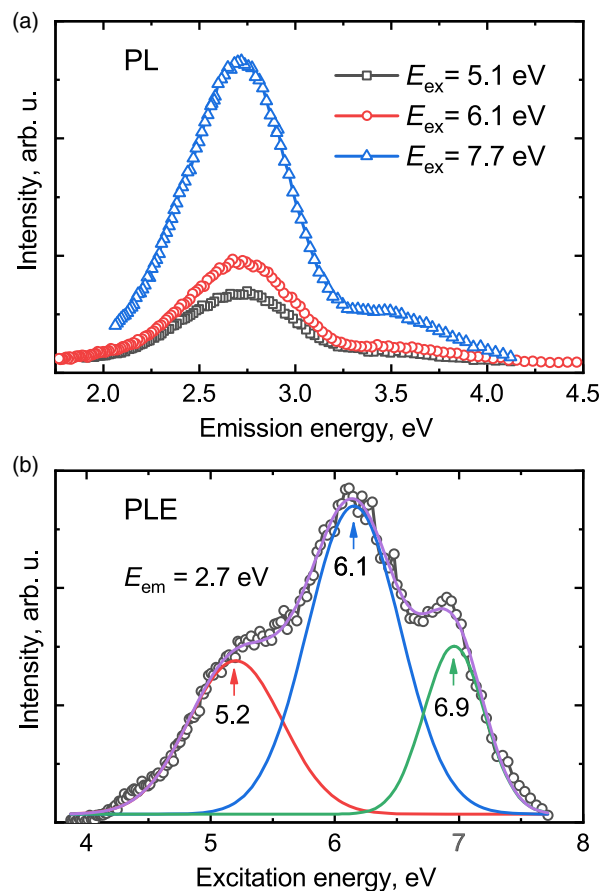


**Figure 5.** Low-temperature PL spectra measured at the excitation by quantum energy a) 5.1, 6.1, and 7.7 eV and b) PLE spectra of the 2.7 eV emission band for OSG low- $\kappa$  films.

to the known optical excitation energy of the Si–Si defect in SiO<sub>2</sub>.<sup>[40–42]</sup> At the same time, the calculated optical absorption peak of 6.1 eV for the oxygen divacancy in the model low- $\kappa$  dielectric structure coincides with the maximum of the blue PL excitation spectrum. Thus, the observed 6.1 eV PLE peaks, as well as the blue PL band, could be caused by oxygen divacancies, but not oxygen vacancies. Note that **Figure 6** shows the spectra for defects with the lowest formation energy, while consideration of all possible positions of defects in the supercell gives a scatter of possible values of optical transition energy  $\pm 0.3$  eV.

The local density of state spatial distribution at the filled defect levels near the valance band top for our simple model low- $\kappa$  structure confirms that the oxygen vacancy and divacancy in the simulated structure form Si–Si and Si–Si–Si bonds, as is the case in SiO<sub>2</sub> (**Figure 6**). The calculated Si–Si bond lengths are 2.349 Å for the monovacancy and 2.366 and 2.372 Å for the divacancy. It shows the similarity of the oxygen vacancy and divacancy electronic structure in the SiCOH low- $\kappa$  dielectric and SiO<sub>2</sub>. In turn, this indirectly justifies the possibility of analyzing the experimental data for a low- $\kappa$  dielectric with the known data for SiO<sub>2</sub>.

There is a rule of thumb that the thermal trap energy in a dielectric coincides with half the Stokes shift of luminescence.

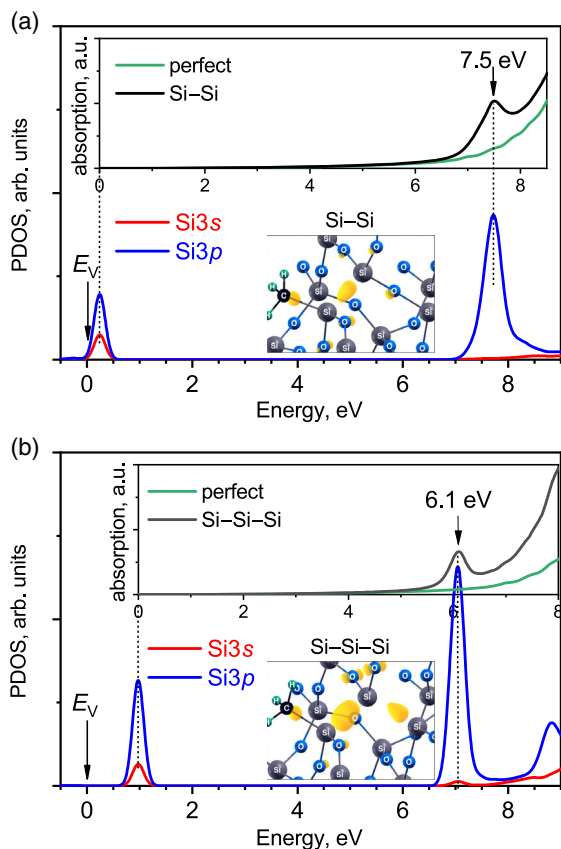


**Figure 6.** Calculated PDOS (bandgap region) of the Si atoms that formed the a) Si–Si defect and b) Si–Si–Si defect: Si 3s, red, and Si 3p, blue.  $E_V$  is the valence band top. The inserts show the corresponding optical absorption spectra and fragments of structures with the distribution of local density of states on filled defects levels (shown in yellow).

This rule holds for many dielectrics, such as  $\text{Si}_3\text{N}_4$ ,  $\text{Al}_2\text{O}_3$ ,  $\text{HfO}_2$ ,  $\text{ZrO}_2$ , and  $\text{Ta}_2\text{O}_5$ .<sup>[51–55]</sup> Guided by this rule, it is easy to estimate the thermal trap energy value of the defect for a studied low- $\kappa$  dielectric based on the Stokes shift of the blue PL. When considering the peak with the energy of 5.2 eV in the PLE spectrum, this estimate will give the  $W_t$  value  $(5.2 - 2.7)/2 = 1.25$  eV, which is close to  $W_t = 1.2$  eV found from the analysis of  $I$ – $V$  characteristics. As discussed previously, the most likely trap with this energy is an oxygen divacancy. For the second peak in the PLE spectrum, the  $W_t$  estimation gives the value  $(6.1 - 2.7)/2 = 1.7$  eV. This value is close to the thermal ionization energy 1.6 eV of the oxygen vacancy in  $\text{SiO}_2$ .<sup>[33]</sup> It is interesting to note that if we take the luminescence with the energy of 3.6 eV for a given PLE peak, we also get  $(6.1 - 3.6)/2 = 1.25$  eV for the  $W_t$  estimation.

Thus, the thermal trap energy values obtained from the Stokes shift of luminescence indirectly confirms the presence of oxygen vacancies and divacancies in the studied low- $\kappa$  films. In addition, the agreement of the thermal energy values obtained from the analysis of luminescence spectroscopy data and the  $I$ – $V$  characteristics confirms the correctness of the N–G model for describing the charge transport mechanism in the studied films.

## 4. Conclusion

In conclusion, the charge transport mechanism and trap nature in simplified OSG (SiCOH) low- $\kappa$  films that contain only terminal methyl groups and are not modified by UV light were investigated. The  $I$ – $V$  characteristics of the studied low- $\kappa$  dielectric films at different temperatures were analyzed using the Frenkel model of thermal ionization of an isolated Coulomb trap in an electric field, the Hill–Adachi model of overlapping Coulomb traps, the Makram-Ebeid and Lannoo model of isolated trap ionization, and the Nasyrov–Gritsenko model of phonon-assisted electron tunneling between neutral traps. The Frenkel model, H–A model, and MA–L model describe the charge transport only when explicitly incorrect fitting parameters are used. Thus, a good agreement with the experiment is provided by the N–G model with the following parameters: thermal trap energy  $W_t = 1.2$  eV, optical energy  $W_{\text{opt}} = 2.4$  eV, effective mass  $m^* = 0.95m_e$ , and trap concentration  $N = 9.4 \times 10^{19} \text{ cm}^{-3}$ . The EELS, as well as PL and PLE spectra, show the presence of oxygen vacancy (Si–Si bond) and divacancy (Si–Si–Si bonds) when we make an analogy with silicon oxide. The electronic structure of oxygen vacancy and divacancy in the simple model low- $\kappa$  SiCOH structure was simulated with DFT. It was found that the oxygen divacancy formation energy is close to that of a pair of distanced vacancies. The calculated projected density of states spectra predicts the possibility of optical transitions on the oxygen divacancy, the energy of which corresponds to the maximum of the excitation spectrum of the blue luminescence band. The thermal trap energy estimation from the luminescence Stokes shift gives a value close to that obtained from the  $I$ – $V$  characteristics simulation, i.e.,  $W_t = 1.2$  eV. Thus, the charge transport through the methyl-terminated OSG low- $\kappa$  dielectric film is described by the N–G phonon-assisted electron tunneling between neutral traps, and traps are the oxygen divacancies with trap energy 1.2 eV.

## Acknowledgements

Experiments and simulation were conducted under the grant of the Russian Foundation for Basic Research (RFBR) (project No. 18-29-27006). The low- $\kappa$  program conceptualization and selection of the material for this research were conducted under the grant RFBR No. 18-29-27022. The recipe development and deposition were conducted under the Ministry of Science and Higher Education of Russia (Nos. FSFZ-2020-0022, FEUZ-2020-0060, 0306-2019-0005). The authors are grateful to the Analytical and Technological Research Center “High Technology and Nanostructured Materials” of NSU. The ab initio computations were carried out at the Novosibirsk State University Supercomputer Center.

## Conflict of Interest

The authors declare no conflict of interest.

## Keywords

charge transport, density functional theory simulations, low- $\kappa$  dielectrics, photoluminescence, trap energy

Received: October 22, 2020  
Revised: November 30, 2020  
Published online: December 21, 2020

- [1] M. R. Baklanov, P. S. Ho, E. Zschech, *Advanced Interconnects for ULSI Devices*, Wiley, Hoboken, NJ **2012**.
- [2] M.R. Baklanov, C. Adelman, L. Zhao, S. De Gendt, *ECSJ. Solid State Sci.* **2015**, 4, Y1.
- [3] A. Grill, *J. Vac. Sci. Technol. B* **2016**, 34 020801.
- [4] Y. F. Lu, R. Ganguli, C. A. Drewien, M. T. Anderson, C. J. Brinker, W. L. Gong, Y. X. Guo, H. Soye, B. Dunn, M. H. Huang, J. I. Zink, *Nature* **1997**, 389, 364.
- [5] P. Van der Voort, D. Esquivel, E. De Canck, F. Goethals, I. Van Driessche, F. J. Romero-Salguero, *Chem. Soc. Rev.* **2013**, 42, 3913.
- [6] K. Maex, M. R. Baklanov, D. Shamiryan, F. Iacopi, S. H. Brongersma, Z. S. Yanovitskaya, *J. Appl. Phys.* **2003**, 93, 8793.
- [7] H. Li, J. M. Knaup, E. Kaxiras, J. J. Vlassak, *Acta Mater.* **2011**, 59, 44.
- [8] J. A. Burg, M. S. Oliver, T. J. Frot, M. Sherwood, V. Lee, G. Dubois, R. H. Dauskardt, *Nat. Commun.* **2017**, 8, 1019.
- [9] C. H. Liu, Q. Qi, D. S. Seregin, A. S. Vishnevskiy, Y. J. Wang, S. H. Wei, J. Zhang, K. A. Vorotilov, F. N. Dultsev, M. R. Baklanov, *Jap. J. Appl. Phys.* **2018**, 57, 07MC01.
- [10] P. Marsik, P. Verdonck, D. De Roest, M. R. Baklanov, *Thin Solid Films* **2010**, 518, 4266.
- [11] M. Krishtab, J. F. de Marneffe, S. De Gendt, M. R. Baklanov, *Appl. Phys. Lett.* **2017**, 110, 013105.
- [12] M. R. Baklanov, L. Zhao, E. Van Besien, M. Pantouvaki, *Microelectron. Eng.* **2011**, 88, 990.
- [13] J. M. Atkin, E. Cartier, T. M. Shaw, R. B. Laibowitz, T. F. Heinz, *Appl. Phys. Lett.* **2008**, 93, 122902.
- [14] J. L. Lauer, J. L. Shohet, Y. Nishi, *Appl. Phys. Lett.* **2009**, 94, 162907.
- [15] E. Van Besien, M. Pantouvaki, L. Zhao, D. De Roest, M. R. Baklanov, Z. Tokei, G. Beyer, *Microelectron. Eng.* **2012**, 92, 59.
- [16] G. B. Alers, K. Jow, R. Shaviv, G. Kooi, G. W. Ray, *IEEE Trans. Device Mater. Reliab.* **2004**, 4, 148.
- [17] J. R. Lloyd, E. Liniger, T. M. Shaw, *J. Appl. Phys.* **2005**, 98, 084109.
- [18] M. R. Baklanov, V. Jousseau, T. V. Rakhimova, D. V. Lopaev, Y. A. Mankelevich, V. V. Afanas'ev, J. L. Shohet, S. W. King, E. T. Ryan, *Appl. Phys. Rev.* **2019**, 6, 011301.
- [19] E. N. Ogawa, O. Aubel, in *Advanced Interconnects For ULSI Devices* (Eds: M. R. Baklanov, P. S. Ho, E. Zschech), Wiley, Hoboken, NJ **2012**, pp. 369–434.
- [20] B. Jinnai, T. Nozawa, S. Samukawa, *J. Vac. Sci. Technol. B* **2008**, 26, 1926.
- [21] M. Krishtab, J. F. De Marneffe, S. Armini, J. Meersschaut, H. Benders, C. Wilson, S. De Gendt, *Appl. Surf. Sci.* **2019**, 485, 170.
- [22] T. Breuer, U. Kerst, C. Boit, E. Langer, H. Ruelke, A. Fissel, *J. Appl. Phys.* **2012**, 112, 124103.
- [23] A. S. Vishnevskiy, D. S. Seregin, K. A. Vorotilov, A. S. Sigov, K. P. Mogilnikov, M. R. Baklanov, *J. Sol-Gel Sci. Technol.* **2019**, 92, 273.
- [24] A. Palov, T. V. Rakhimova, M. B. Krishtab, M. R. Baklanov, *J. Vac. Sci. Technol. B* **2015**, 33, 020603.
- [25] P. Giannozzi, O. Andreussi, T. Brumme, O. Bunau, M. B. Nardelli, M. Calandra, R. Car, C. Cavazzoni, D. Ceresoli, M. Cococcioni, N. Colonna, I. Carnimeo, A. Dal Corso, S. de Gironcoli, P. Delugas, R. A. DiStasio, A. Ferretti, A. Floris, G. Fratesi, G. Fugallo, R. Gebauer, U. Gerstmann, F. Giustino, T. Gorni, J. Jia, M. Kawamura, H. Y. Ko, A. Kokalj, E. Kucukbenli, M. Lazzeri, et al., *J. Phys.-Condens. Mat.* **2017**, 29, 465901.
- [26] J. Frenkel, *Phys. Rev.* **1938**, 54, 647.
- [27] K. A. Nasyrov, V. A. Gritsenko, *J. Appl. Phys.* **2011**, 109, 093705.
- [28] K. A. Nasyrov, V. A. Gritsenko, *Phys.-Uspehi* **2013**, 56, 999.
- [29] R. M. Hill, *Philos. Mag.* **1971**, 23, 59.
- [30] H. Adachi, Y. Shibata, S. Ono, *J. Phys. D: Appl. Phys.* **1971**, 4, 988.
- [31] S. S. Makram-Ebeid, M. Lannoo, *Phys. Rev. B* **1982**, 25, 6406.
- [32] C. Wu, Y. Li, A. Lesniewska, O. V. Pedreira, J. F. de Marneffe, I. Ciofi, P. Verdonck, M. R. Baklanov, J. Bommels, I. De Wolf, Z. Tokei, K. Croes, *J. Appl. Phys.* **2015**, 118, 164101.
- [33] D. R. Islamov, V. A. Gritsenko, T. V. Perevalov, O. M. Orlov, G. Y. Krasnikov, *Appl. Phys. Lett.* **2016**, 109, 052901.
- [34] R. A. B. Devine, W. L. Warren, J. B. Xu, I. H. Wilson, P. Paillet, J. L. Leray, *J. Appl. Phys.* **1995**, 77, 175.
- [35] S. L. Miller, D. M. Fleetwood, P. J. Mcwhorter, *Phys. Rev. Lett.* **1992**, 69, 820.
- [36] D. Z. Gao, J. Strand, M. S. Munde, A. L. Shluger, *Front Phys.* **2019**, 7, 43.
- [37] M. S. Munde, D. Z. Gao, A. L. Shluger, *J. Phys.: Condens. Matter.* **2017**, 29, 245701.
- [38] P. Lazzeri, L. Vanzetti, M. Anderle, M. Bersani, J. J. Park, Z. Lin, R. M. Briber, G. W. Rubloff, H. C. Kim, R. D. Miller, *J. Vac. Sci. Technol. B* **2005**, 23, 908.
- [39] T. V. Perevalov, D. R. Islamov, *Microelectron. Eng.* **2019**, 216, 111038.
- [40] H. Imai, K. Arai, H. Imagawa, *Phys. Rev. B* **1988**, 38, 12772.
- [41] R. Tohmon, Y. Shimogaichi, H. Mizuno, Y. Ohki, K. Nagasawa, Y. Hama, *Phys. Rev. Lett.* **1989**, 62, 1989.
- [42] L. Skuja, *J. Non-Cryst. Solids* **1998**, 239, 16.
- [43] V. S. Kortov, A. F. Zatsepin, S. V. Gorbunov, A. M. Murzakaev, *Phys. Solid State* **2006**, 48, 1273.
- [44] K. Raghavachari, D. Ricci, G. Pacchioni, *J. Chem. Phys.* **2002**, 116, 825.
- [45] L. N. Skuja, A. N. Streletsky, A. B. Pakovich, *Solid State Commun.* **1984**, 50, 1069.
- [46] L. S. Liao, X. M. Bao, X. Q. Zheng, N. S. Li, N. B. Min, *Appl. Phys. Lett.* **1996**, 68, 850.
- [47] J. Y. Zhang, X. M. Bao, N. S. Li, H. Z. Song, *J. Appl. Phys.* **1998**, 83, 3609.
- [48] S. Agnello, R. Boscaino, M. Cannas, F. M. Gelardi, M. Leone, B. Boizot, *Phys. Rev. B* **2003**, 67, 033202.
- [49] K. Awazu, H. Kawazoe, K. Muta, *J. Appl. Phys.* **1991**, 70, 69.
- [50] V. S. Kortov, A. F. Zatsepin, V. A. Pustovarov, A. A. Chudinov, D. Y. Biryukov, *Radiat. Meas.* **2007**, 42, 891.
- [51] V. A. Gritsenko, T. V. Perevalov, O. M. Orlov, G. Y. Krasnikov, *Appl. Phys. Lett.* **2016**, 109, 062904.
- [52] V. A. Pustovarov, V. S. Aliev, T. V. Perevalov, V. A. Gritsenko, A. P. Eliseev, *J. Exp. Theor. Phys.* **2010**, 111, 989.
- [53] V. A. Gritsenko, T. V. Perevalov, D. R. Islamov, *Phys. Rep.* **2016**, 613, 1.
- [54] T. V. Perevalov, D. V. Gulyaev, V. S. Aliev, K. S. Zhuravlev, V. A. Gritsenko, A. P. Yelissev, *J. Appl. Phys.* **2014**, 116, 244109.
- [55] V. A. Gritsenko, T. V. Perevalov, V. A. Voronkovskii, A. A. Gismatulin, V. N. Kruchinin, V. S. Aliev, V. A. Pustovarov, I. P. Prosvirin, Y. Roizin, *ACS Appl. Mater. Interface.* **2018**, 10, 3769.